Structure of the ripple phase of phospholipid multibilayers

Kheya Sengupta,[1,*] V. A. Raghunathan,[1,†] and John Katsaras[2,‡]
[1]*Raman Research Institute, Bangalore 560 080, India*
[2]*National Research Council, Steacie Institute for Molecular Sciences, Building 459, Station 18, Chalk River, Ontario, Canada K0J 1J0*
(Received 10 May 2003; published 29 September 2003)

We present electron density maps (EDMs) of the ripple phase formed by phosphorylcholine lipids such as dimyristoyl phosphatidylcholine (DMPC), palmitoyl-oleoyl phosphatidylcholine (POPC), dihexadecyl phosphatidylcholine, and dilauroyl phosphatidylcholine (DLPC). With the exception of DLPC, the rippled bilayers have a sawtooth shape in all the systems, with one arm being almost twice as long as the other. For DMPC and POPC bilayers, EDMs have been obtained at different temperatures at a fixed relative humidity, and the overall shape of the ripples and the ratio of the lengths of the two arms are found to be insensitive to temperature. EDMs of all the systems with saturated hydrocarbon chains suggest the existence of a mean chain tilt along the ripple wave vector. In the literature it is generally assumed that the asymmetry of the rippled bilayers (absence of a mirror plane normal to the ripple wave vector) arises from a sawtoothlike height profile. However, in the case of DLPC, the height profile is found to be almost symmetric and the asymmetry results mainly from different bilayer thicknesses in the two arms of the ripple. We also present EDMs of the metastable ripple phase of dipalmitoyl phosphatidylcholine, formed on cooling from the L_α phase.

DOI: 10.1103/PhysRevE.68.031710 PACS number(s): 61.30.Eb, 61.10.Eq

I. INTRODUCTION

Phospholipids are amphiphilic molecules with a hydrophilic head group and one or more hydrophobic hydrocarbon chains. They self-assemble in water to form a variety of thermodynamic phases, depending upon the temperature and water content [1]. Many phospholipids show lamellar phases consisting of stacks of bilayers separated by water. In the L_α phase found above the chain melting transition temperature, the chains are molten and the positional order in the plane of the bilayer is liquidlike. Such fluid bilayers have been widely studied as model biomembranes. In the lower temperature gel (L_β or $L_{\beta'}$) phase the chains are predominantly in the all-*trans* conformation and the in-plane positional order is at least quasi-long-range [2,3]. In the $L_{\beta'}$ phase the chains are tilted with respect to the layer normal, whereas in the L_β phase there is no such tilt. At high water content some phospholipids such as phosphatidylcholines also exhibit a modulated phase in between the L_α and $L_{\beta'}$ phases [1,2,4]. This is the $P_{\beta'}$ or ripple phase, characterized by a one-dimensional periodic height modulation of the bilayers.

X-ray and freeze fracture experiments show the existence of two types of ripple phases. The commonly reported phase is thermodynamically stable and has a wavelength of about 150 Å [1,4,5]. X-ray diffraction patterns from this phase can be indexed on a two dimensional oblique lattice ($\gamma \neq \pi/2$). These rippled bilayers lack a mirror plane normal to the ripple wave vector, and are often referred to as asymmetric ripples [1,6–9]. In addition, metastable ripples are sometimes seen while cooling from the L_α phase [5,10,11]. Their wavelength is about twice that of the coexisting stable ripples. Diffraction patterns from metastable ripples can be indexed on a two-dimensional rectangular lattice ($\gamma = \pi/2$). Freeze fracture studies indicate a symmetric height profile (with a mirror plane normal to the ripple wave vector) for these metastable ripples [6].

The tilt of the hydrocarbon chains with respect to the local layer normal plays an important role in many theories of the ripple phase. For example, the Lubensky-MacKintosh model [12,13] forbids a tilt along the rippling direction and the Seifert-Shillcock-Nelson model [14] is based on the idea that tilts in the two leaflets of the bilayer (i.e., in the two monolayers that make up the bilayer) are weakly coupled. However, details of chain packing in the ripple phase have not yet been well established experimentally. Though the lipid hydrocarbon chains are generally assumed to be mostly rigid and to lie on a hexagonal lattice [2,4], diffusion and nuclear magnetic resonance experiments indicate that there is considerable disorder associated with the chain region [15,16]. The nature of this disorder is still a matter of debate. Empirically, only lipids that have an $L_{\beta'}$ phase at lower temperatures are found to exhibit the ripple phase [17], indicating the importance of chain tilt in the formation of ripples [18]. An exception is dihexadecyl phosphatedylcholine (DHPC), which has an interdigitated gel phase rather than a $L_{\beta'}$ phase below the ripple phase [19], resulting from a head group cross-sectional area that is much larger than that of two chains. Since in the ripple phase of DHPC the chains do not interdigitate, a nonzero chain tilt is very likely. However, thus far it has not been possible to unambiguously determine the magnitude and direction (with respect to the ripple wave vector) of chain tilt directly from x–ray diffraction patterns of any phospholipid system forming rippled bilayers. The reason for this is that the chain reflections are rather diffuse, possibly the combined result of disordered chains and the rippling of the bilayers themselves.

Sun *et al.* [8] have calculated an electron density map

*Present address: Physik Department E22, TU Muenchen, 85747 Garching, Germany.
Electronic address: ksengupt@physik.tu-muenchen.de
†Electronic address: varaghu@rri.res.in
‡Electronic address: john.katsaras@nrc.ca

(EDM) of the asymmetric ripple phase of dimyristoyl phosphatidylcholine (DMPC) from the x-ray data of Wack and Webb [20]. Their main findings were the following.

(a) The rippled bilayers have a sawtooth height profile.

(b) Bilayer thickness is smaller in the shorter arm of the sawtooth and is comparable to the bilayer thickness in the L_α phase; bilayer thickness in the longer arm is found to be about the same as that in the $L_{\beta'}$ phase.

(c) The electron density in the head group region in the shorter arm is lower than that in the longer arm, and their ratio is comparable to the ratio of electron densities in the head group regions of the L_α and $L_{\beta'}$ phases. Based on these observations, they proposed a working hypothesis that hydrocarbon chains in the longer arm of the ripple are extended, similar to those in the $L_{\beta'}$ phase, whereas in the shorter arm, the chain conformation resembles that in the L_α phase.

This L_α-$L_{\beta'}$ microphase separation hypothesis put forward by Sun *et al.* [8] is incompatible with many experimental observations. For example, though self-diffusion in the ripple phase is found to be highly anisotropic, with a fast component that is four to five orders of magnitude faster than the slow component, the fast component itself is about two to three orders of magnitude smaller than self-diffusion in the L_α phase [16]. Thus the authors of Ref. [16] concluded that although intramolecular hydrocarbon chain disorder might be substantial in the fast bands, intermolecular order in this region is not like that in the L_α phase. Another compelling evidence against the microphase separation hypothesis comes from calorimetric studies [21]. The ratio of the lengths of the two arms of the ripple as observed in the EDM is about 1:2. Therefore, according to the microphase separation picture, about 2/3 of the chains become all-*trans* at the $L_\alpha \rightarrow P_{\beta'}$ transition (main transition). The rest of the chains can go to the all-*trans* conformation either gradually, thus giving rise to a temperature dependence of the ratio of the lengths of the two arms, or abruptly at the $P_{\beta'} \rightarrow L_{\beta'}$ transition (pretransition). Our experiments (discussed below) rule out any significant temperature dependence of the lengths of the two arms. Then according to the microphase separation model, 1/3 of the chains should go to the all-*trans* conformation at the pretransition. This would imply that the ratio of the latent heat of the main transition to that of the pre transition should be roughly 2:1. But the observed ratio is about 10:1. Further, latent heat of pretransition is found to be essentially independent of chain length for a given head group [20]. Thus the microphase separation picture is incompatible with diffusion and calorimetric experiments.

We have recently proposed an alternative interpretation of the EDM of the asymmetric ripple phase of DMPC [9]. In this picture, differences in bilayer thickness, and head group electron densities in the two arms of the ripple, arise mainly from a nonzero mean tilt of the chains along the ripple wave vector. We have determined the EDMs of the ripple phase of a few different phospholipids in order to gain some insight into the structure of this phase. We have also studied two of the systems at different temperatures to see if the ratio of the lengths of the two arms depends on temperature. Our main finding is that the structure of the ripple phase of all lipids studied are very similar, with a larger bilayer thickness in the longer arm of the ripple. Most of the EDMs are consistent with the presence of a mean chain tilt along the ripple wave vector. Moreover, contrary to what is generally assumed, we find that the asymmetry of the ripples arises primarily from different bilayer thicknesses in the two arms and not from an asymmetric height profile.

Although the basic structural features of the stable asymmetric ripple phase have now been well established, there is some ambiguity even about the bilayer shape in the metastable ripple phase [22–27]. Freeze fracture experiments indicate that the rippled bilayers in this phase have grooves along their maxima [25–27]. Since the method of three-dimensional reconstruction from freeze fracture data is not very accurate, the existence of the groove is not well established. X-ray data from multidomain samples are also difficult to analyze because of the coexistence of the two kinds of ripples. It has also been suggested that x-ray diffraction patterns from samples cooled from the L_α phase can be indexed on a single two-dimensional lattice, instead of two lattices corresponding to the coexisting stable and metastable phases [23,24]. However, such an interpretation is not consistent with freeze fracture observations and with the results of a recent x-ray diffraction study using aligned dipalmitoyl phosphatodylcholine (DPPC) multibilayers [11]. With a view to clarify the situation, we have also calculated EDMs of the metastable symmetric ripple phase of DPPC from x-ray data on oriented samples. The quality of these maps is not as good as those of the stable asymmetric phase. If, as indicated by freeze fracture experiments, the structure of this phase lacks a center of symmetry, then this may be at least partly due to the difficulty in phasing the reflections arising from such a structure. However, we are able to obtain certain features of this phase, which have been hitherto unknown.

II. EXPERIMENTAL

We have studied both the asymmetric and symmetric ripple phases formed by a number of phosphorylcholine lipid systems. For asymmetric ripples, we have analyzed data from three sources.

(1) Data from unoriented samples of DMPC obtained using a synchrotron source, reported by Wack and Webb [20].

(2) Data from aligned bilayer stacks of DMPC, POPC (palmitoyl-oleoyl phosphatidylcholine), DHPC, and mixtures of DPPC and DHPC collected by us using a rotating anode x-ray generator.

(3) Data from unoriented samples of dilauroyl phosphatidylcholine (DLPC) reported by Tardieu *et al.* [1]. Other data available in the literature have too many overlapping reflections to be suitable for our present analysis. For the symmetric ripples, we have analyzed data from fully hydrated aligned samples of DPPC obtained using synchrotron radiation [11].

A locally built temperature and humidity controlled heater was used to collect data from oriented samples [28]. All lipids studied were obtained from either Sigma-Aldrich (St. Louis, MO) or Avanti Polar Lipids (Alabaster, AL) and were used without further purification. Samples were prepared by

spraying a solution of the lipid in methanol on the convex surface of a glass beaker (radius ≈ 1.5 cm). The solvent was then evaporated off under vacuum and the lipid was hydrated by keeping the beaker in a humid atmosphere for a minimum of 12 h. The sample was then transferred to the heater. Humidity was maintained by placing a suitable saturated salt solution inside the airtight chamber of the heater and allowing it to equilibrate. Temperature was controlled by using a circulating water bath. The sample was cycled up and down through the main and pretransitions a few times to facilitate hydration and alignment. This method of sample preparation orients the bilayers parallel to the substrate, but does not fix the ripple direction. Thus each bilayer consists of many domains, with the orientation of the ripples varying from domain to domain. The x-ray beam was tangential to the substrate and we assume that the scattering volume contained a large number of domains so that their distribution with respect to the ripple direction can be taken to be uniform.

Normally, in order to obtain many reflections, an oriented sample has to be rotated while being exposed to x rays. The lipid bilayer systems studied here give rise to only a rather small number of reflections, due to the large degree of disorder present in them. The curvature of the orienting substrate introduces artificially the ''mosaicity'' that is required to obtain simultaneously all the reflections from these systems. Further, the fact that each bilayer consists of randomly oriented ripple domains makes the sample effectively unoriented in the plane of the bilayer. This is equivalent to rotating the sample about an axis parallel to the bilayer normal and perpendicular to the beam direction. Thus the method of sample preparation used by us dispenses with the need to rotate the samples [29]. Geometric and absorption corrections for the present sample geometry are discussed in the Appendixes.

Cu K_α ($\lambda = 1.54$ Å) radiation from a rotating anode x-ray generator (Rigaku) operating at 50 kV and 80 mA and rendered monochromatic by a flat graphite monochromator was used to illuminate the sample. The diffraction patterns were collected by an image plate (x-ray research). Locally written programs (using the image handling routines pg plot) were used to extract the intensities of the reflections.

III. PHASING THE REFLECTIONS

Only the magnitudes of the structure factors ($|F_{\mathbf{q}}|$) are available from x-ray diffraction data, but in order to calculate an EDM we also need their phases. Based on previous observations [1,8], the structure is assumed to belong to the centrosymmetric plane group $p2$. The structure factors in this case are real and the phases are constrained to be either 0 or π. To determine the phases we have used a modeling and least squares fitting procedure first employed by Sun *et al.* [8] in the context of the $P_{\beta'}$ phase. In this approach, a function representing the electron density in one unit cell of the lattice is first constructed, such that it incorporates known and plausible features of the structure. This function has free parameters built into it to account for the imprecisely known features. This trial function is Fourier transformed to calculate the structure factors. The values of these parameters are

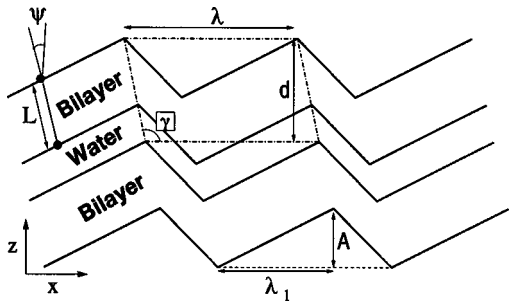

FIG. 1. Schematic showing the structural parameters of the ripple phase.

determined by a standard least squares fitting procedure, where the calculated magnitudes of the structure factors are fitted to the observed ones. The calculated structure factors corresponding to the final fitted parameters yield the phases of the reflections. These phases are combined with the observed structure factor magnitudes and inverse Fourier transformed to get the EDM.

The electron density within a unit cell, $\rho(x,z)$, is described as the convolution of a ripple contour function $C(x,z)$ and the transbilayer electron density profile $T_\psi(x,z)$: $\rho(x,z) = C(x,z) * T_\psi(x,z)$. In reciprocal space the convolution becomes a simple multiplication. The structure factor $F(\mathbf{q})$ is, therefore, given by $F(\mathbf{q}) = F_C(\mathbf{q}) F_T(\mathbf{q})$, where $F_C(\mathbf{q})$ and $F_T(\mathbf{q})$ are the Fourier transforms of $C(x,z)$ and $T_\psi(x,z)$, respectively. The ripple contour function is written as $C(x,z) = \delta(z - u(x))$, where $u(x)$ describes the ripple profile. $u(x)$ is taken to have the form of a sawtooth with peak-to-peak amplitude A_r. λ_1 is the projection of the longer arm of the sawtooth on the x axis (Fig. 1). A_r and λ_1 are adjustable parameters. To check if the final shape is an artifact of the specific initial model, a smoother initial shape given by $u(x) = a \sin(qx) + b \sin(2qx)$ was also tried. Here a and b are the adjustable parameters. $T_\psi(x, z)$ gives the electron density at any point (x, z) in the bilayer along a straight line, which makes an angle ψ with the z axis. Electron density in the methylene region of the bilayer is close to that of water and is taken as zero. We have used three models for $T_\psi(x, z)$, models I and II being equivalent to the simple delta function (SDF) and modified Gaussian (M1G) models of Ref. [8], respectively.

Model I. Here $T_\psi(x,z)$ is taken as consisting of two δ functions with positive coefficients ρ_H, corresponding to the head group regions separated by a distance L, and a central δ function with negative coefficient of magnitude ρ_M corresponding to the methyl region. The variable head-to-head distance L accounts for both chain melting and a tilt in the direction perpendicular to the rippling direction. There are six adjustable parameters in this model. They are A_r, λ_1, ψ, L, ρ_H/ρ_M, and an overall normalization factor.

Model II. In this more realistic model, the δ functions representing the head and methyl groups are replaced by Gaussians of width σ_h and σ_m, respectively. The electron density in the minor arm is allowed to be different by a factor of f_1 from that in the major arm. The region where the two arms meet is modeled as a wall with the electron density differing by a factor of f_2 from the rest of the arm. The wall

thickness is fixed at a value that is small compared to the bilayer thickness, half of the wall region being in each arm. There are ten adjustable parameters in this model.

Model III. In models I and II, the head-to-head distance L is fixed along a direction making an angle ψ with respect to the z axis. This forces the bilayer thickness along the layer normal to be different in the two arms. Therefore in model III, these restrictions are lifted and the parameters L, ψ, σ_h, σ_m, and ρ_H/ρ_M, are allowed to be different in the two arms of the ripple. Further, the wall between the two arms is taken to have a variable width w. This model has 15 adjustable parameters. Minimization was done by iterative least squares fitting with respect to six variables at a time.

The values of the adjustable parameters in the models discussed above are determined by a nonlinear least squares fitting procedure that uses the Levenberg-Marquardt method [30]. The final converged values of the parameters are put back into the expression for F^{hk} to get the best-fit structure factors F_c^{hk}. The phase Φ_c^{hk} of the reflection with indices (h,k) is $F_c^{hk}/|F_c^{hk}| = \pm 1$ (since the structure is assumed to be centrosymmetric). The product of the observed structure factor magnitude ($|F_o^{hk}|$) and Φ_c^{hk} gives $F(\mathbf{q})$, which is then inverse Fourier transformed to get the EDM.

We have analyzed the data of Ref. [20] using all three models for electron density described above. As discussed below, in this case all three models lead to essentially identical EDMs. Data from oriented samples collected by us could be analyzed only using model I. Models II and III have many more adjustable parameters in them and they did not converge to any reasonable limit. The lack of convergence is presumably due to errors in the intensities of the reflections, arising from the approximations involved in the geometric and absorption corrections to the intensity, applicable in the present geometry (see Appendixes).

We have also calculated EDMs of the metastable ripple phase using data from an oriented sample of DPPC. The diffraction patterns clearly show the coexistence of two ripple phases, one with $\gamma \neq \pi/2$ and the other with $\gamma = \pi/2$ [11]. The bilayer periodicity d, wavelength λ, and the angle γ of the former are comparable to those of the phase obtained on heating the sample from the $L_{\beta'}$ phase. Therefore, we identify this phase as the stable asymmetric phase. The corresponding parameters of the other phase with $\gamma = \pi/2$ are comparable to those reported for the metastable ripple phase. The use of an oriented sample makes it possible to clearly distinguish the reflections arising from the two coexisting phases. Hence it is clear that all the reflections in the diffraction pattern do not arise from a single two-dimensional structure as proposed in Refs. [23,24].

The EDMs of the metastable phase were also calculated using the modeling procedure discussed above. For the transbilayer profile, $T_\psi(x,z)$, model I was used. For the ripple profile, $C(x,z)$, different shapes shown in Fig. 2 were tried. The simplest choice for $C(x,z)$ is the sawtooth that is also used to phase reflections from asymmetric ripples [Fig. 2(a)]. As the projected length of the longer arm is a variable, this can also model a triangular shape. We have also used a triangular profile with grooves at both extrema for the ripple shape [Fig. 2(c)]. Since these two profiles are centrosymmetric, phases of the reflections are constrained to be either 0 or π. Freeze fracture electron microscopic studies [26,27] indicate the ripple profile to be triangular with grooves only at one set of extrema [Fig. 2(b)]. This structure is noncentrosymmetric and hence the structure factors are in general complex. When we use this shape for the ripple profile, the parameters in the model for electron density do not converge, presumably due to the fact that the phases can now have values in the entire range 0–2π. While using this profile, therefore, we fixed all the parameters except the groove depth A_d at values obtained using the centrosymmetric profile [Fig.2(c)]. This was followed by iterative least square fits of each of these variables taken one at a time till the variations from one fit to the next were negligible.

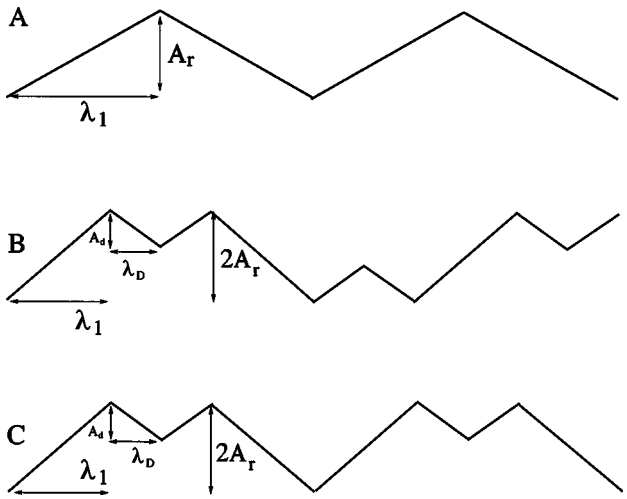

FIG. 2. The ripple profiles in the (a) 0-groove (b) 2-groove and (c) 1-groove models.

IV. RESULTS AND DISCUSSION

A. DMPC

DMPC has a phosphatidylcholine head group and two saturated 14 C atoms long hydrocarbon chains that are attached to the backbone by ester linkages. Data from Ref. [20] were fitted using the three models for $T_\psi(x,z)$ [9] and result in the same phases for all the reflections except for the faint $(0, k)$ and $(3, 0)$ reflections. Model III gives only a marginally better fit than model II. The values of L in the two arms are almost the same and comparable to that obtained from model II. This is also true for other parameters, which are allowed to be different in the two arms. However, model III gives a slightly higher value (0.7) for f_1. As discussed below, this factor can be accounted for in terms of the chain tilt, without assuming a L_α-like organization in the minor arm. The low $\Sigma(=\Sigma_{h,k}||F_c^{hk}|-|F_o^{hk}||^2)$ and $R[=(\Sigma_{h,k}\|F_c^{hk}|-|F_o^{hk}\|)/\Sigma_{h,k}|F_o^{hk}|]$ values for models II and III, and the absence of any physically unacceptable features in the EDM (Fig. 3) indicate that these models closely represent the intrinsic structure of the system. The resulting EDM is shown in Fig. 3. This map is essentially the same as that presented in Ref. [8] since, as mentioned above, the set

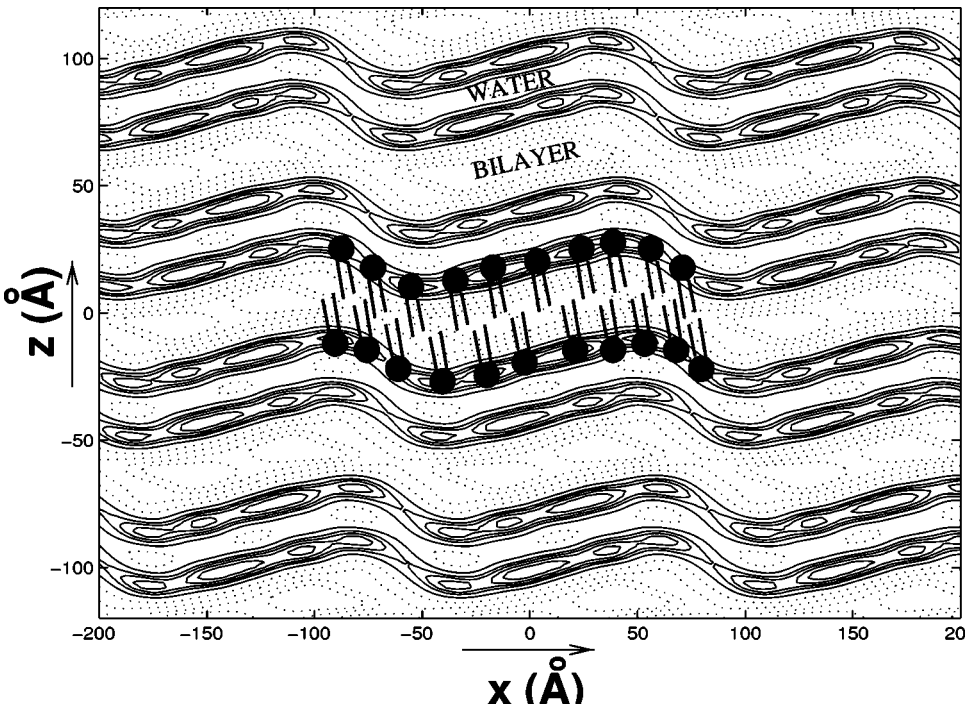

FIG. 3. Electron density map of the ripple phase of DMPC. $T = 18.2\,^{\circ}\mathrm{C}$ and partial specific volume of water = 0.263 (data from Ref. [20]). Note that the thickness of the bilayers is about 40 Å, whereas that of the water region is about 15 Å. The figure also shows a schematic of the proposed arrangement of lipid molecules in the rippled bilayers.

of phases obtained using models I and II (that were also used in [8]) are essentially the same as those obtained using model III.

It is clear from Fig. 3 that the ripples have a sawtooth shape, with an offset between the two leaflets of the bilayer. The simplest explanation for this offset is an average tilt of the chains along the rippling direction; such an offset cannot be expected if the tilt were in a plane normal to the rippling direction. The tilt angle ψ is found to be approximately equal to $(\gamma\text{-}\pi/2)$. Further support for an average tilt along this direction comes from the fact that the value of L is almost equal in the two arms and is comparable to twice the length of a fully stretched DMPC molecule. However, as pointed out by Nagle [31], the value of L ($\sim$37 Å) is about 5 Å smaller than the head-to-head bilayer thickness expected from the $L_{\beta'}$ bilayers [3]. Therefore, we have to invoke some degree of conformational disorder of the chains in order to account for the observed bilayer thickness.

If the chains are assumed to be tilted at an angle ψ to the z axis, their tilt with respect to the local layer normal can be calculated from the ripple shape, using, $\theta_{1(2)} = \psi - (+)\arctan(A_r/\lambda_{1(2)})$, where the subscripts 1 and 2 correspond to the longer and shorter arm, respectively. Using values of the structural parameters reported earlier [9], θ_1 and θ_2 turn out to be $\sim 0^{\circ}$ and $\sim 35^{\circ}$, respectively. The tilt in the shorter arm is comparable to that found in the $L_{\beta'}$ phase. Since the area per molecule is inversely proportional to the cosine of this angle, a value of 0.82 is obtained for f_1. This is in very good agreement with the value of 0.77 obtained from the map for the ratio of the average electron densities in the head group region of the longer and shorter arms. Thus an average tilt of the chains along the rippling direction provides a consistent explanation for many of the features in the electron density profile. This means that the height modulation of the bilayers along the x axis can be described as arising from a relative sliding movement of neighboring chains, with all the chains lying in the x-z plane and tilted by a constant angle ψ with respect to the z axis (Fig. 3).

If the ripple profile is taken to be smoother, given by, $u(x) = a\sin(qx) + b\sin(2qx)$, we find that the final electron density map is unaffected. But if the initial shape is very different from the actual shape, for example, if $u(x)$ is chosen to be a simple sinusoidal function, then the fit is poor and the final electron density map contains many unphysical features such as discontinuity of bilayers. Thus, as expected, the modeling procedure seems to work only if the initial model is somewhat close to the actual electron density distribution in the system.

We have calculated EDMs of the ripple phase of DMPC at different temperatures and constant relative humidity (98%), using data from oriented films [9]. Structural features of the ripples are found to be similar to those of Ref. [20]. In particular, θ_1 and θ_2 are close to 0° and 30°, respectively, for all the temperatures studied. Temperature dependence of the structural parameters is found to be very weak (Table I), as in the case of DPPC [32]. Contrary to results of freeze fracture experiments [7], we find that at all temperatures, the ripple shape has Fourier components higher than the second.

TABLE I. The structural parameters of the $P_{\beta'}$ phase of DMPC at different temperatures and 98% RH.

$T(^{\circ}\mathrm{C})$	d (Å)	λ_r (Å)	γ (deg)
25	55.6±0.1	140±2	99±1
24	55.8	142	99
23	55.9	142	100
22	56.0	144	100
21	56.3	145	99
20	56.4	154	99

TABLE II. Converged values of the model parameters for DMPC at different temperatures and 98% RH. The tilt angle in the two arms of the ripple are also given.

T(°C)	25	24	23	22	21	20
λ_1 (Å)	89.8	91.3	87.8	87.5	94.9	97.6
A_r (Å)	19.4	19.6	19.2	19.2	20.5	20.3
ψ (deg)	5.7	5.7	11.4	5.7	5.7	2.8
ρ_H/ρ_M	1.4	1.5	1.4	1.5	1.6	1.5
L (Å)	40.2	40.2	40.2	40.2	40.2	40.2
θ_1 (deg)	−3	−3	−2	−2	−3	−2
θ_2 (deg)	30	30	29	28	31	29

Further, we do not find a significant temperature dependence of the amplitude of the ripples, again in contrast to the results of Ref. [7]. The converged values of the fitted parameters are given in Table II. The values of Σ and R for these fits are about 3500 and 0.3, respectively. Note that the values of L, given in the table, are obtained using model I and are comparable to the head-to-head distance expected from gel phase data; however, the more detailed models give a lower value of L [9].

B. POPC

The molecular structure of POPC differs from that of DMPC, as the two hydrocarbon chains in the former are of unequal lengths, being 16 and 18 C atoms long. Further, the longer chain contains a double bond halfway through its length. The electron density map of oriented rippled POPC bilayers at two temperatures and 75% RH is shown in Fig. 4. The structural parameters are given in Table III and the converged values of the model parameters in Table IV. For these fits, the values of Σ and R are about 1000 and 0.3, respectively. The angle γ is much larger than in the case of DMPC bilayers, whereas the wavelength and layer spacing are comparable. As reported in Ref. [9], structural features of the rippled POPC bilayers vary significantly with temperature, unlike those of DMPC. The layer spacing decreases slowly and γ increases steadily as temperature is increased. The ripple wavelength first decreases and then suddenly increases to a large value just below the main transition. These trends are very similar to those seen in DPPC [32], but in POPC the temperature dependence is much more pronounced. As in DMPC, the rippled bilayers in POPC have a sawtooth shape. The peak-to-peak amplitude, except near the L_α transition, is about 10 Å, half that of DMPC. Table IV also gives the tilt angles θ_1 and θ_2 in the two arms of the ripple, calculated using the values of ψ obtained from the fit. Note that in this case the values of ψ are very different from $(\gamma\text{-}\pi/2)$. If the latter values are used to calculate the tilt angles, then θ_1 turns out to be $\sim 20°$ and not ~ 0. This along with the fact that the value of L in this case is not comparable to twice the molecular length, makes it impossible to get any information about chain packing from the EDMs. The double bond in one of the chains of the POPC molecule leads to a kink in the chain when it is in the fully stretched conformation, resulting in a lower main transition temperature. It is interesting that this feature does not seem to affect the gross structure of the $P_{\beta'}$ phase. It is likely that the terminal region of the chain beyond the double bond is always in a molten conformation, as proposed by Cevc [33].

C. DHPC

The only difference between the molecular structures of DMPC and DHPC is that in the latter the hydrocarbon chains are connected to the backbone through ether rather than ester linkages. The crystallographic parameters of the ripple phase at 37 °C and 95±2% RH are: $\lambda_r = 140.9$ Å, $d = 62.3$ Å, and $\gamma = 100°$. The temperature dependence of these parameters is negligible. An EDM calculated using data from an oriented sample, is given in Fig. 5. It can be seen that the general shape is again a sawtooth with two unequal arms and suggests a tilt of the chains along the rippling direction. The converged values of the model parameters are $A_r = 20.5$ Å, $\lambda_1 = 96.2$ Å, $\psi = 9.6°$, $L = 46.2$ Å, $\rho_H/\rho_M = 1.0$. The value of L in this case is close to the expected head-to-head bilayer thickness. Further, the tilt angles θ_1 and θ_2 are $-2°$ and 34°, respectively, and almost identical to the corresponding values for DMPC. Σ and R for this fit are about 5000 and 0.6, respectively. In all the compounds discussed so far, that is, DMPC, POPC, and DHPC, the ratio of the lengths of the major and minor arms is about 2 and this ratio is essentially insensitive to temperature. As mentioned earlier, this observation contradicts the view that chain organization in the minor arm is similar to that found in the L_α bilayers.

D. Mixture of DHPC and DPPC

The phase diagram of mixtures of DHPC and DPPC has been studied by Lohner *et al.* [19]. These mixtures exhibit the $P_{\beta'}$ phase over a larger temperature range compared to the pure systems; the range being maximum (≈ 20 °C) for the 1:1 mixture. We have studied the temperature dependence of the structural parameters in the 1:1 (wt %) mixture, using oriented samples. Although there were too few reflections, probably due to inherent disorder in the system, for calculating an EDM, the crystallographic parameters could still be computed and are given in Table V. The values of these parameters for the mixture are close to those observed in the pure systems. The layer spacing d and the angle γ are insensitive to variations in temperature, whereas the wavelength decreases from a large value near the pretransition to a value comparable to that in DPPC at higher temperatures.

E. DLPC

DLPC is similar to DMPC except that its hydrocarbon chains are shorter and are made up of 12 C atoms each. We have phased the data of Tardieu *et al.* [1] from an unoriented sample at −7 °C containing 77 wt % water. The lattice parameters are $\lambda_r = 85.3$ Å, $d = 51.9$ Å, and $\gamma = 110°$. Figure 6 shows a map calculated using our modeling and fitting approach. The converged values of the model parameters are $A_r = 11.5$ Å, $\lambda_1 = 39.4$ Å, $\psi = 18.2°$, $L = 34.6$ Å, $\rho_H/\rho_M = 1.2$. For this fit the values of Σ and R are about 100 and 0.2, respectively. The set of phases obtained by us leads to a

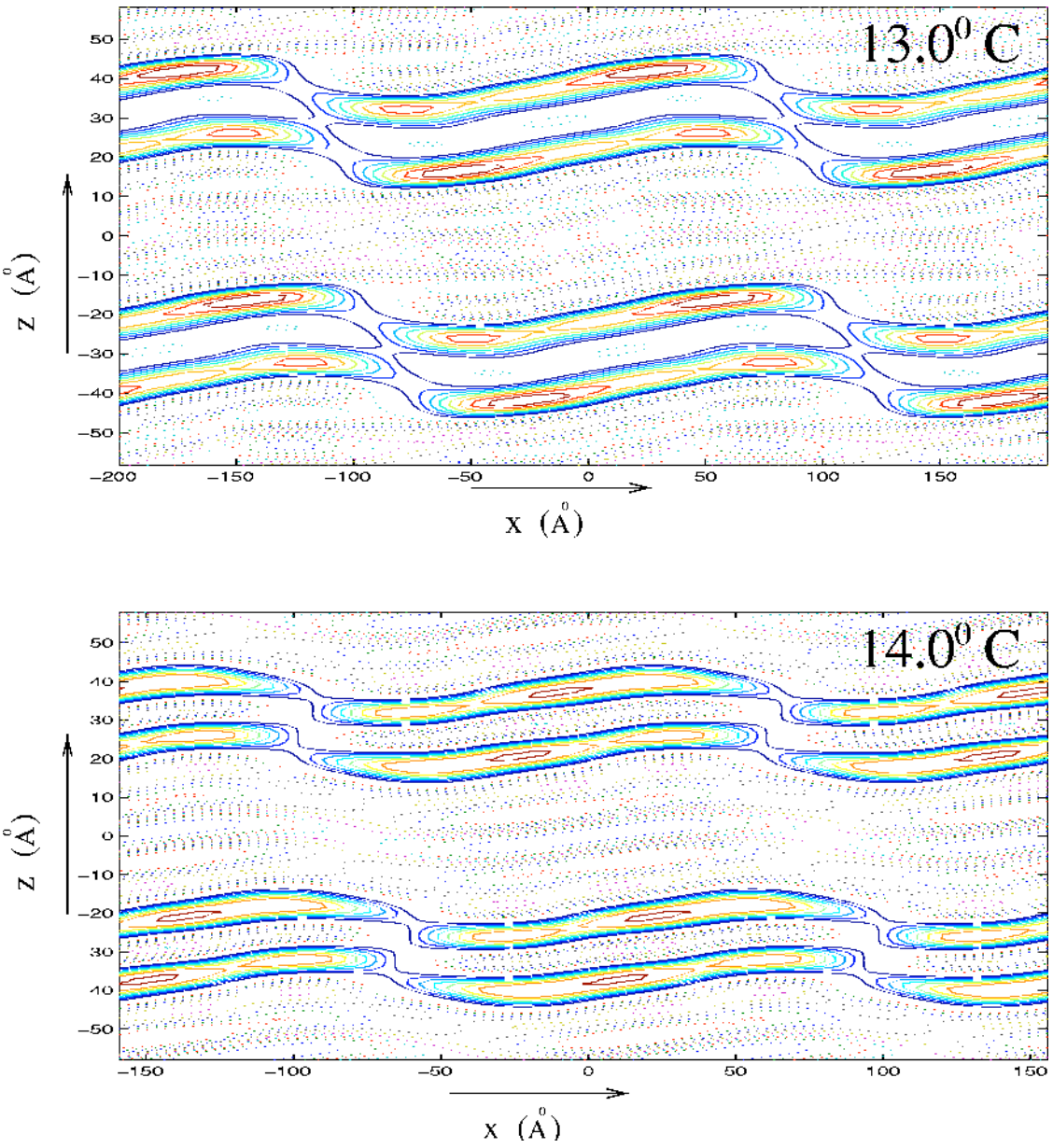

FIG. 4. Electron density map of the $P_{\beta'}$ phase of POPC at two temperatures at 75% RH.

better EDM compared to that reported in Ref. [1]. The bilayers in this case have a triangular shape. The major and minor arms are more or less of equal length. But the ripple profile still lacks a mirror plane normal to the rippling direction as the bilayer thickness is not the same in the two arms. Electron density in the head group region is again higher in the thicker arm and the value of the model parameter L is comparable to twice the length of a fully stretched DLPC molecule (32.6 Å). Thus the structure of this system is also consistent with the presence of an average chain tilt along the rippling direction. From the values of the structural parameters we can estimate the chain tilt angle with respect to the local layer normal to be 3° in the thicker arm and 33° in the thinner one. Note that these values are consistent with the chain packing model proposed from the DMPC data.

TABLE III. Temperature variation of the structural parameters of the ripple phase of POPC at 75% RH.

T(°C)	d (Å)	λ_r (Å)	γ (deg)
13.0	58.3±0.1	200±2	116±1
13.5	58.0	170	119
14.0	58.0	159	120
14.5	57.3	143	124
15.0	56.4	266	133

F. Chain packing in the bilayers

As discussed above, EDMs of the asymmetric ripple phase of all lipids studied, except POPC, suggest the existence of an average chain tilt along the ripple wave vector. The tilt angle of the chains with respect to the local bilayer

TABLE IV. Converged values of the model parameters for the ripple phase of POPC at 75% RH. The tilt angle in the two arms of the ripple are also given.

T(°C)	λ_1 (Å)	A_r (Å)	ψ (deg)	ρ_H/ρ_M	L (Å)	θ_1 (deg)	θ_2 (deg)
13.0	169.0	15.9	0.0	1.3	38.8	−5	27
13.5	127.3	13.9	0.5	1.5	50.4	−5	19
14.0	121.7	12.0	0.6	1.4	51.2	−5	19

normal turns out to be about 0° in the longer arm and about 30–35° in the shorter arm, in all of these cases. It is known that in the crystalline phase of hydrocarbons, where the chains are in the all-*trans* conformation, tilt of the chains arises because of relative shifting of adjacent chains along their axes by one zigzag unit of the fully stretched chain. Thus, knowing the separation between the chains and the length of one zigzag unit, one can estimate the angle of tilt. Assuming that the chain tilt in lipids arise in a similar fashion, the expected tilt in the $L_{\beta'}$ phase can be estimated to be $\approx 30°$ (taking the lateral separation of the chains to be ≈ 4 Å). This is very close to the value we obtain in the thinner arm of the ripple and also, to the reported values of the tilt angle in the $L_{\beta'}$ phase which is usually in the range 30°–35°. This variation of the tilt angle along the ripple vector (alternating between ~ 0 and $\sim 30°$), is very similar to that proposed by Larsson [34].

In the case of POPC the tilt angles in the two arms do not follow the above trend, and the value of L does not match the length of the molecule. As mentioned earlier, one of the hydrocarbon chains in POPC has a double bond, unlike all other lipids studied here, which have only fully saturated chains. It is possible that the different behavior exhibited by POPC is a consequence of the presence of the unsaturated chain. Further work is needed to clarify this point.

It is well known that the hydrocarbon chains in lipids tilt because of the size mismatch between the head groups and the chains [35,36]. If the chains are not tilted, bulky head groups force the interchain spacing to be larger than the value preferred by the chains. By tilting, acyl chains can reduce the interchain distance to its optimum value, while allowing for the head group separation to be larger. Thus, a chain tilt in the gel phase indicates a larger head group separation compared to the interchain distance and the absence of tilt indicates a smaller head group spacing. Alternatively, if the chain conformation is not all-*trans*, the chain cross-sectional area is larger and again the tilt can be expected to be zero. Therefore, we may conclude that, in the thicker (major) arm of the ripples, either the head group conformation is different from that in the thinner arm or the chains are not in the all-*trans* conformation and have some degree of disorder, thus increasing the effective chain cross-sectional area. The present data are insufficient to distinguish between these two possibilities. Conventionally, such a chain disorder is thought to arise because of the presence of *gauche* conformations along the chains. An intriguing alternative scenario is that, in the ripple phase, the stretched chains in the longer arm rotate about their long axis, thus increasing their effective cross-sectional area, as in the ''rotor'' phase of long chain hydrocarbons [37].

G. Origin of the ripple asymmetry

As mentioned earlier, rippled bilayers lack a mirror plane normal to the ripple wave vector. The origin of this asymme-

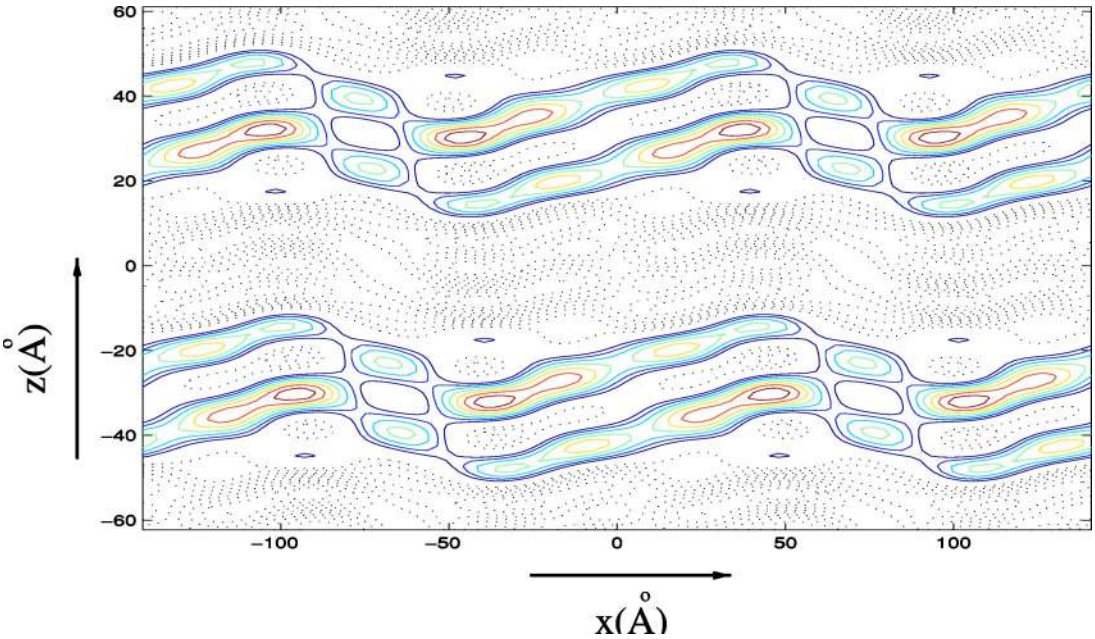

FIG. 5. Electron density map of the $P_{\beta'}$ phase of DHPC at 37 °C and 97% RH.

TABLE V. Temperature dependence of the ripple parameters in a 1:1 (wt %) mixture of DHPC and DPPC at 95% RH.

T(°C)	d (Å)	λ_r (Å)	γ (deg)
26	60±2	175±5	94±2
30	60	157	94
34	62	147	98
38	62	151	99
42	58	132	95

try has been the subject of many recent studies. Lubensky and MacKintosh proposed that the chirality of the molecules was responsible for asymmetry [12,13]. However, later experiments showed that this was not the case [38]. Seifert *et al.* have suggested that it arises from the locking of the tilts in the two leaflets of the bilayer at a nonzero value [14]. Dipolar interactions between bilayers have also been invoked to explain the asymmetry [39]. All of these theories assume that the asymmetry of the bilayers is due to their asymmetric height profile. It is clear from the EDMs presented above that, in general, there are two causes for the bilayer asymmetry: (a) an asymmetric height profile as envisaged in the theories and (b) difference in the bilayer thickness in the two arms of the ripple. In most of the systems these two features coexist. However, in the case of DLPC we find that the asymmetry arises only from the second cause, whereas the height profile itself is almost symmetric. Thus, it seems that the difference in the bilayer thickness of the two arms is the primary cause of asymmetry of the rippled bilayers, and can be theoretically modeled as arising from a mean chain tilt along the ripple wave vector [40].

The unit cell parameters of the ripple phase of DLPC have also been reported by Wack and Webb [20] under somewhat similar conditions as Tardieu *et al.* [1]. However, the values

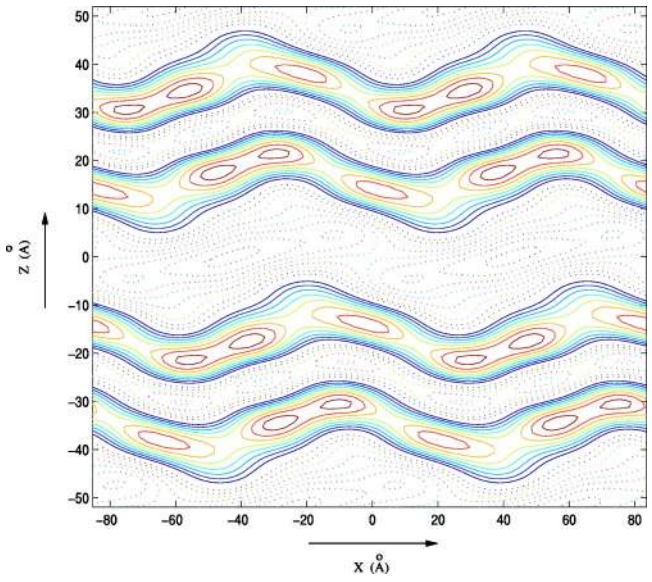

FIG. 6. EDM of the $P_{\beta'}$ phase of DLPC at −7°C and 77 wt % water, using the phases calculated by the modeling procedure described in the text. (data from Ref. [1])

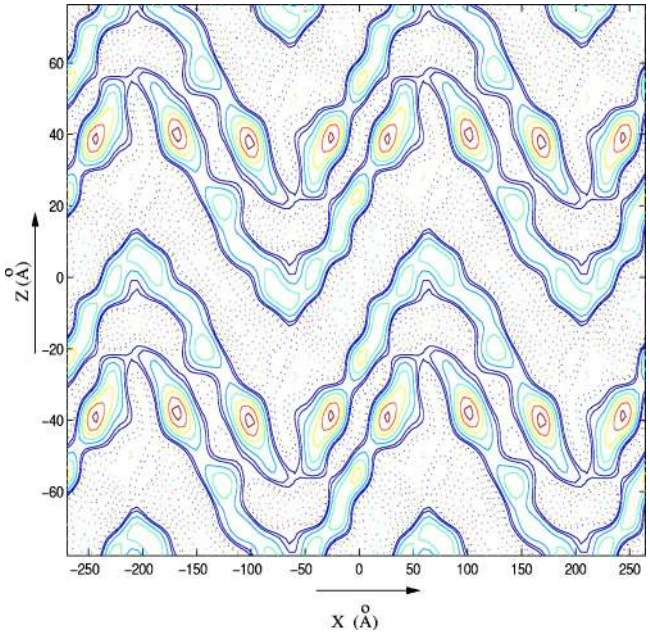

FIG. 7. EDM of the metastable ripple phase of DPPC at 39.2 °C and 100% RH obtained using the triangular wave profile. The positive (negative) contours are represented by solid (dotted) lines. The regions with positive electron density correspond to the head groups.

of these parameters obtained by them are significantly different. For example, the ripple wavelength and γ found by Wack and Webb [20] are about 110 Å and 100°, respectively, compared to 85 Å and 110° reported in Ref. [1]. The origin of this discrepancy is presently not clear. However, the data of Tardieu *et al.* [1] clearly establish the importance of the difference in the bilayer thickness in the two arms, in the formation of the asymmetric ripple phase.

H. EDM of the metastable ripple phase

None of the three shapes shown in Fig. 2 leads to a good fit between the calculated and observed structure factors, and hence the EDMs are not of very good quality. Both centrosymmetric shapes yield EDMs where the top and bottom leaflets of the bilayers have different shapes near the peaks (Fig. 7). Since this does not seem very plausible, we surmise that the structure is probably noncentrosymmetric. Even with the noncentrosymmetric shape shown in Fig. 2(c), we still do not get a good fit. However, as discussed earlier, this may be due to the difficulty in phasing the reflections from such a structure, the structure factors in this case being complex. When using this shape, we have held all parameters, other than the groove width and depth, at values obtained from the other shapes. We have also tried fixing the values of ripple amplitude A_r and groove depth A_d at those obtained from freeze fracture experiments [27]. But EDMs corresponding to values close to these are found to be unphysical. The best EDM that could be obtained is given in Fig. 8.

The overall shape of the bilayers is similar to that obtained using the centrosymmetric models. The peak-to-peak amplitude is about 50 Å and the water layer thickness is

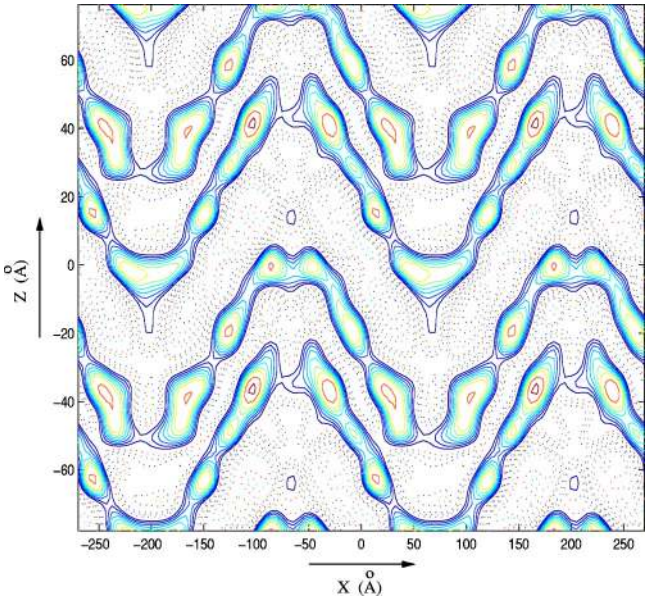

FIG. 8. EDM of the metastable ripple phase of DPPC at 39.2°C and 100% RH obtained using the 1-groove model.

probably more than that in the asymmetric phase, as suggested in Ref. [11]. The higher water content points to enhanced long-range interbilayer repulsion in the metastable phase, either of electrostatic origin or due to the Helfrich interaction [41] arising from thermal undulations of the bilayers. However, if the chains are mostly all–*trans*, the bilayers would be rigid and the Helfrich interaction would be negligible. On the other hand, the only possible source of electrostatic interactions is through the dipolar head groups. Since the conformation of the head groups in the two kinds of ripples are not known, the details of dipolar interactions cannot be further commented upon. Thus, further work is needed to clarify the origin of higher water layer thickness in the metastable phase.

V. CONCLUSIONS

We have calculated electron density maps of the ripple phase of DMPC, POPC, DHPC, and DLPC. The shape of the ripples in these systems are very similar and all of them exhibit asymmetric ripples that lack a mirror plane normal to the ripple wave vector. We do not see any temperature dependence of the ripple shape, though the values of the structural parameters do vary with temperature. EDMs of the ripple phase of all lipids studied, except POPC, are consistent with the existence of an average chain tilt in the direction of rippling. The height profile of the bilayers in DMPC, POPC, and DHPC has a sawtooth shape. The width of the minor arm is comparable to the bilayer thickness in all the systems. In DLPC, the height profile is closer to triangular with the width of the two arms being almost equal and comparable to the bilayer thickness. Finally, from the EDM of DLPC it is clear that the difference in the bilayer thickness of the two arms of the ripple is the primary cause of asymmetry of the bilayers in the ripple phase, a fact that seems to not have been previously appreciated.

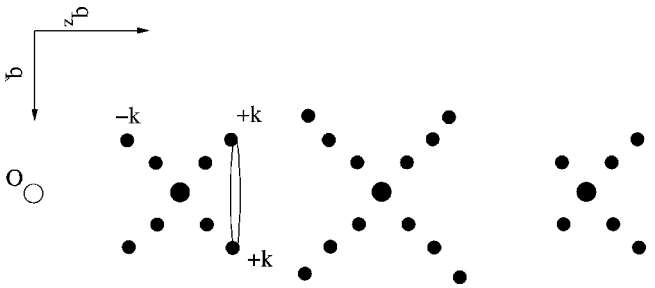

FIG. 9. Schematic diagram of a typical diffraction pattern from the ripple phase. The open circle marked "o" corresponds to the origin. The big filled circles are the main reflections and the small filled circles are the satellites. Each satellite is a ring in the reciprocal space, which cuts the Ewald sphere twice thus giving rise to two spots.

We have also calculated electron density maps of the metastable symmetric ripples of DPPC that are sometimes formed on cooling from the L_α phase. The amplitude is about 50 Å and is in agreement with that estimated from freeze fracture experiments. The shape of the ripples near the peaks is poorly resolved, but the structure is probably noncentrosymmetric with a groove at the peak.

ACKNOWLEDGMENT

We thank M. Mani for technical assistance.

APPENDIX A: GEOMETRIC CORRECTIONS

In this appendix we discuss the geometric corrections needed for the intensities of the reflections in the diffraction pattern of the ripple phase obtained from oriented multilayers. Let us first consider an ideal fully aligned planar sample, so that the normal to the bilayers is along z and the ripple wave vector is along x. The reciprocal lattice of this structure would consist of a set of "main" reflections $(h, 0)$ along q_z and a set of "satellite" reflections (h, k), $k \neq 0$ in the q_x-q_z plane. As discussed earlier, it is not possible to align the ripple direction through out the sample and each bilayer consists of many domains, which differ in the direction of the ripple wave vector. We shall assume that the scattering volume consists of a large number of such domains, so that the ripple wave vectors of these domains can be taken to be uniformly distributed in the x-y plane. As a result, the satellite reflections now become rings in the q_x-q_y plane. Reflections present in the diffraction pattern correspond to the intersection of these rings with the Ewald sphere, each ring thus giving rise to two equivalent reflections (Fig. 9).

We now take into account the influence of the curvature of the cylindrical substrate which introduces an effective mosaicity of the sample. We shall consider its effect on the main and satellite reflections separately. As a result of substrate curvature, the main reflections become arcs that subtend an angle Δ at the origin of the reciprocal space. Since Δ is the same for all the reflections, the smearing out is more for larger scattering angles (Fig. 10). This leads to a large reduction in the observed intensity of the reflections. To correct for this effect, the observed intensity has to be multiplied by the

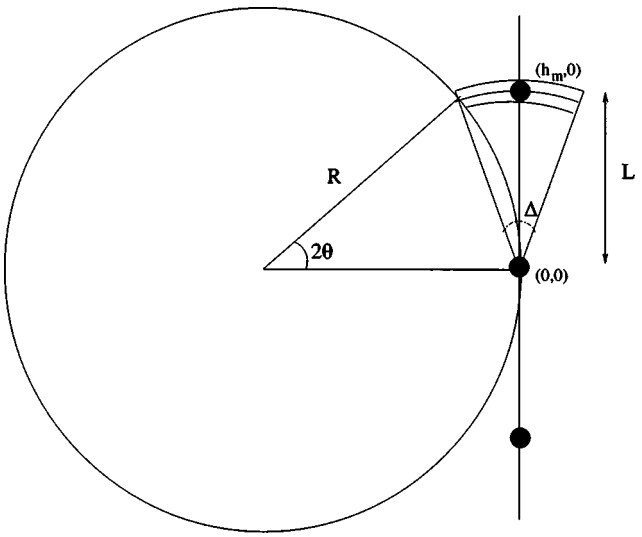

FIG. 10. Geometrical correction for the main reflections. $(h_m,0)$ is the highest order main reflection detected. The circle of radius $R=2\pi/\lambda$ represents the Ewald sphere. The angular spread of the $(h, 0)$ reflections is Δ. This corresponds to a linear spread of $L\Delta$, where L is the distance (in reciprocal space) between the mth order and the origin; $L=4\pi \sin\theta/\lambda$. From simple geometric constructions, the condition for the mth order reflection, corresponding to a Bragg angle θ_m, to intersect the Ewald sphere is $\Delta=2\theta_m$. To estimate L, it is assumed that the angular spread in the $L_{\beta'}$ and $P_{\beta'}$ phases is the same. The highest order reflection visible in the $L_{\beta'}$ phase is the 8th order. This gives a lower limit for L, since it is possible that higher order reflections are present but are too faint to be detected. Another way of estimating L is from the fact that for the highest order recorded, the angle Δ is given by $\cos\Delta=(r-w)/r$, where r is the radius of the beaker and w is the beam-width (≈ 1 mm). The two estimates are comparable and typical, $\Delta\approx 10°$.

length of the arc which is given by $(4\pi/\lambda)\ \Delta \sin\theta$, where λ is the wavelength of the incident x rays and θ is the corresponding Bragg angle. This arc has a finite width and what is recorded is the cross section of this with the Ewald sphere. As the Ewald sphere cuts the arc at an angle θ, a further factor of $\cos\theta$ is present. The corrected intensity is given by

$$I_c = I_o \frac{4\pi}{\lambda} \Delta \sin\theta \cos\theta, \tag{A1}$$

where I_o and I_c are the observed and corrected intensities; see Fig. 10 for an explanation of how Δ is estimated.

The mosaicity introduced by the curvature of the substrate also smears out the satellite reflections. If the mosaicity is not large enough, it merely increases the cross-sectional area of the rings in the reciprocal space. Note that in this case it is not necessary to correct for the substrate curvature, since the Ewald sphere intersects the smeared out rings in the reciprocal space, resulting in somewhat broadened reflections. However, as this ring intersects the Ewald sphere at a small angle there is a correction factor given by the cosine of the angle, which is negligible at the small angles we are interested in.

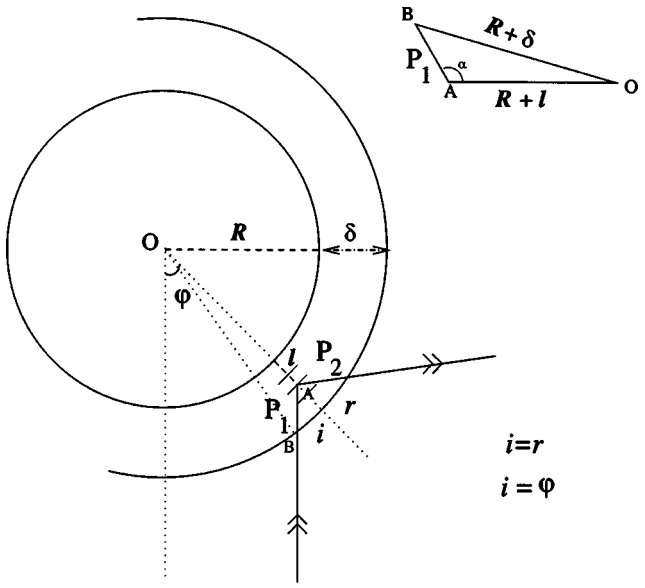

FIG. 11. Calculation of the path traveled by the x-ray beam inside the sample. R is the radius of the beaker and δ is the sample thickness. P_1 and P_2 are the paths traveled by x rays (marked by double arrow) before and after reflection from the sample. To calculate P_1, the triangle OAB is considered. From geometrical considerations, the Bragg angle $\theta=\pi/2-\phi$ and $\alpha=\pi-\phi$. Therefore, applying rules of trigonometry to triangle OAB, P_1 is given by $-(R+l)\sin(\theta)+[(R+\delta)^2-(R+l)\cos^2(\theta)]^{1/2}$. Since the rays are Bragg reflected, from laws of reflection and geometry it can be shown that, $P_2=P_1$. Therefore, $p(l)=2P_1(l)$.

The observed intensity has to be multiplied by the perimeter of the ring to get the total intensity. The radius of this ring is $(2\pi|k|/\lambda_r)\sin\gamma$, where k is the corresponding Miller index and γ is the angle between the basis vectors. Therefore, for the satellite reflections,

$$I_c = I_o \frac{4\pi^2}{\lambda_r} |k| \sin\gamma. \tag{A2}$$

Note that the corrections for main and satellite reflections are different in the present sample geometry, unlike in the cases of fully oriented and fully unoriented samples [42]. Therefore, all the numerical factors in the above two equations cannot be neglected.

APPENDIX B: ABSORPTION CORRECTIONS

In the present geometry, unlike in conventional powder samples, different parts of the samples diffract into different orders. Therefore, the path traveled inside the medium and hence the absorption correction is different for each reflection. The total path traveled by the x-ray beam diffracted from each part of the sample is calculated from geometrical considerations. The linear absorption coefficient μ is estimated (from the values of the atomic absorption coefficients given in standard tables and using the volumetric data of Wiener *et al.* [43]) to be equal to 9 cm^{-1}. The absorption corrected intensity is given by

$$I_c = I_o \delta \Big/ \left(\int_0^{\delta} e^{-\mu p(l)} dl \right), \tag{B1}$$

where $p(l)$ is the path traveled by the x rays inside the medium [see Fig. 11 for the expression for $p(l)$] and δ is the sample thickness.

Since the sample thickness is difficult to measure, we have not been able to take absorption corrections into account. To check if this omission seriously affects our final electron density maps, we have assumed some reasonable values for the thickness (of the order of 10 to 100 μm) and applied the corrections. We find that the final electron density map is not affected in any significant way by these corrections.

[1] A. Tardieu, V. Luzzati, and F.C. Reman, J. Mol. Biol. **75**, 711 (1973).

[2] G.S. Smith, E.B. Sirota, C.R. Safinya, and N.A. Clark, Phys. Rev. Lett. **60**, 813 (1988); G.S. Smith, E.B. Sirota, C.R. Safinya, R.J. Plano, and N.A. Clark, J. Chem. Phys. **92**, 4519 (1990).

[3] W.-J. Sun, R.M. Suter, M.A. Knewtson, C.R. Worthington, S. Tristram-Nagle, R. Zhang, and J.F. Nagle, Phys. Rev. E **49**, 4665 (1994).

[4] M.J. Janiak, D.M. Small, and G.G. Shipley, J. Biol. Chem. **254**, 6068 (1979).

[5] P. Pinta da Silva, J. Microsc. **12**, 185 (1971); A.J. Verkleij, P.H.J. Ververgaert, L.L.M. Van Deenen, and P.F. Elbers, Biochim. Biophys. Acta **288**, 326 (1972); P.H.J. Ververgaert, A.J. Verkleij, P.F. Elbers, and L.L.M. Van Deenen, *ibid.* **311**, 320 (1973).

[6] D. Ruppel and E. Sackmann, J. Phys. (Paris) **44**, 1025 (1983).

[7] J.T. Woodward, IV and J.A. Zasadzinski, Phys. Rev. E **53**, R3044 (1996).

[8] W.-J. Sun, S. Tristram-Nagle, R.M. Suter, and J.F. Nagle, Proc. Natl. Acad. Sci. U.S.A. **93**, 7008 (1996).

[9] Kheya Sengupta, V.A. Raghunathan, and John Katsaras, Europhys. Lett. **49**, 722 (2000).

[10] H. Yao, S. Matuoka, B. Tenchov, and I. Hatta, Biophys. J. **59**, 252 (1991).

[11] J. Katsaras, S. Tristram-Nagle, Y. Liu, R.L. Headrick, E. Fontes, P.C. Mason, and J.F. Nagle, Phys. Rev. E **61**, 5668 (2000).

[12] T.C. Lubensky and F.C. MacKintosh, Phys. Rev. Lett. **71**, 1565 (1993).

[13] C.-M. Chen, T.C. Lubensky, and F.C. MacKintosh, Phys. Rev. E **51**, 504 (1995).

[14] U. Seifert, J. Shillcock, and P. Nelson, Phys. Rev. Lett. **77**, 5237 (1996).

[15] R.J. Wittebort, C.F. Schmidt, and R.G. Griffin, Biochemistry **20**, 4223 (1981).

[16] M.B. Schneider, W.K. Chan, and W.W. Webb, Biophys. J. **43**, 157 (1983).

[17] D.M. Small, *Handbook of Lipid Research: The Physical Chemistry of Lipids From Alkanes to Phospholipids* (Plenum Press, New York, 1986).

[18] S. Kirchner and G. Cevc, Europhys. Lett. **28**, 31 (1994).

[19] K. Lohner, A. Schuster, G. Degovics, K. Muller, and P. Laggner, Chem. Phys. Lipids **44**, 61 (1987).

[20] D.C. Wack and W.W. Webb, Phys. Rev. A **40**, 2712 (1989).

[21] J.M. Carlson and J.P. Sethna, Phys. Rev. A **36**, 3359 (1987).

[22] S. Matuoka, H. Yao, S. Kato, and I. Hatta, Biophys. J. **64**, 1456 (1993).

[23] M. Rappolt and G. Rapp, Eur. Biophys. J. **24**, 381 (1996).

[24] P.C. Mason, B.D. Gaulin, R.M. Epand, G.D. Wignall, and J.S. Lin, Phys. Rev. E **59**, 3361 (1999).

[25] D. Ruppel and E. Sackmann, J. Phys. (Paris) **44**, 1025 (1983).

[26] E. Sackmann, D. Ruppel, and C. Gebhardt, in *Liquid Crystals of One and Two Dimensional Order*, edited by W. Helfrich and G. Heppke (Springer-Verlag, Berlin, 1980).

[27] J.A.N. Zasadzinski and M.B. Schneider, J. Phys. (Paris) **48**, 2001 (1987).

[28] J. Katsaras and M.J. Watson, Rev. Sci. Instrum. **71**, 1737 (2000).

[29] J. Torbet and M.H.F. Wilkins, J. Theor. Biol. **62**, 447 (1976).

[30] W.H. Press, S.A. Teukolsky, W.T. Vellerling, and B.P. Flannery, *Numerical Recipes* (Cambridge University Press, Cambridge, 1997).

[31] J. F. Nagle (private communication).

[32] Y. Inoko, T. Mitsui, K. Ohki, T. Sekiya, and Y. Nozawa, Phys. Status Solidi A **61**, 115 (1980).

[33] G. Cevc, Biochemistry **30**, 7186 (1991).

[34] K. Larsson, Chem. Phys. Lipids **20**, 225 (1977).

[35] D.J. Vaughan and K.M. Keough, FEBS Lett. **47**, 158 (1974).

[36] F. Jahnig, K. Harlos, H. Vogel, and H. Eibl, Biochemistry **18**, 1459 (1979).

[37] D. Marsh, Biochemistry **19**, 1632 (1980).

[38] J. Katsaras and V.A. Raghunathan, Phys. Rev. Lett. **74**, 2022 (1998); K. Sengupta, V.A. Raghunathan, and J. Katsaras, Phys. Rev. E **59**, 2455 (1999).

[39] C. Misbah, J. Duplat, and B. Houchmandzadeh, Phys. Rev. Lett. **80**, 4598 (1998).

[40] K. Sengupta, V.A. Raghunathan, and Y. Hatwalne, Phys. Rev. Lett. **87**, 055705 (2001).

[41] W. Helfrich, Z. Naturforsch. **33a**, 305 (1978).

[42] M.J. Buerger, *Crystal-Structure Analysis* (Wiley, New York, 1960).

[43] M.C. Wiener, R.M. Suter, and J.F. Nagle, Biophys. J. **55**, 315 (1989).